Nanoscale

Unveiling the shape-diversified silicon nanowires made by HF/HNO3 isotropic etching with the assistance of silver

Journal:	*Nanoscale*
Manuscript ID:	NR-ART-10-2014-005949.R2
Article Type:	Paper
Date Submitted by the Author:	18-Nov-2014
Complete List of Authors:	Chen, Chia-Yun; Department of Applied Materials and Optoelectronic Engineering, National Chi Nan University Wong, C; Georgia Institute of Technology, Department of Materials Science and Engineering

SCHOLARONE™
Manuscripts

Cite this: DOI: 10.1039/c0xx00000x

www.rsc.org/xxxxxx

ARTICLE TYPE

Unveiling the shape-diversified silicon nanowires made by HF/HNO_3 isotropic etching with the assistance of silver

Chia-Yun Chen,*[a] and Ching-Ping Wong[b,c]

Received (in XXX, XXX) Xth XXXXXXXXX 20XX, Accepted Xth XXXXXXXXX 20XX

DOI: 10.1039/b000000x

Hydrofluoric (HF) / nitric (HNO_3) / acetic (CH_3COOH) acid, normally referred as HNA method, has been considered a most widely utilized technique for performing the isotropic etching on silicon (Si) in industrial Si-based processing and device construction. Here, we reported the novel etching strategy based on HF/HNO_3 process with the assistance of silver (Ag) nano-seeds, offering the well controllability of preparing the diversified Si nanostructure arrays with particularly smooth top surfaces. The involving mechanism was visualized by systematically investigating both the time and temperature dependences on etching kinetics with various ratios of HF to HNO_3. Moreover, by testing different Ag^+-ion containing oxidants on Si etching, we have re-examined the state-of-art metal-assisted chemical etching (MaCE) using HF/$AgNO_3$ etchants. Contradicted with the previous reports, we found that the interplay of hole injections from Ag^+ an NO_3^- ions to the valence band of Si collectively contributes to the unidirectional dissolution of Si, Finally, we explored the engineering of the Ag nano-seeds to regularize the orientation of etched nanowires formed on non-Si (100) wafers, which further provides the reliable pathway for constructing the desired morphologies of one-dimensional Si nanostructures regardless of wafer orientations.

Introduction

Bulk silicon (Si) etching techniques, emerged the selective removal of Si from bulk substrates, have been broadly applied in the fabrication of solid-state electronics, micromachining sensors, and optoelectronic devices.[1,2] Among them, hydrofluoric/nitric/acetic acids (HNA) method is the most widely utilized technique in industrial Si-based processing,[3] mainly because of its process rapidity and simplicity beyond many other dry etching routes. Starting from Robbins and Schwartz in 1959 while performing electrochemical etching of Si in the mixed solutions using HNA method,[4] this technique has bonded with well compatibility of on-chip circuitry and even provided the flexible micrometer-scale machining capacity in diverse applications. In general, HNA etching involves with the oxidation of Si driven by NO species and followed by the removal of soluble silicon compounds initiated with HF etchant. Unfortunately, the etching profile via HNA processing is inevitably limited to the isotropic dissolution of Si and with no preference of particular crystal planes.[3,4] More critically, this process encounters the intrinsic difficulty of scaling down the etching dimensionality toward nanoscale, which radically impedes their practical applications for many nano-sized functional devices.

Recently, metal-assisted chemical etching (MaCE) has been intensively studied for preparing low-dimensional Si nanostructures,[5] paving the way for the realization of unprecedented material properties in bulk Si.[6] In fact, MaCE process emerges the local oxidation of Si assisted by metal catalyst and subsequent dissolution of oxidized Si by HF etchants, where these two fundamental criteria on reacting with Si approach to the essential route of Si dissolution through HF/HNO_3 process. Such unexpected similarity, which has not been explored yet, may further address the feasibility of modified HF/HNO_3 method on dimensional processing of Si with nanometer-scale control, and significantly enlarge the applicable fields of HNA techniques, especially for realizing the nanodevices with enhanced performance and even revolutionary properties. Therefore, in this study, systematical investigations of new designed HF/HNO_3 etching of Si with the assistance of Ag were performed, ranging from structural characterizations, surface wettability, etching kinetics and were further extended to the orientation-dependent morphological transition of formed nanowires. The current work is also of great importance to explore the universal understanding of related MaCE process. In fact, we further unveiled the electrochemical process of reported one-step MaCE, where the distinct etching mechanism was visualized to remedy the unidirectional dissolution of Si.

Experimental section

Substrate Preparation

Three various single crystalline p-type Si wafers, (100), (110) and (111), with resistivity of 1 to 10 Ω cm were utilized to conduct etching experiments. Prior to etching process, Si wafers were

ultrasonically cleaned using acetone, isopropyl alcohol and DI water with several cycles. For the preparation of surface-passivated Si substrates, the cleaned Si wafers were dipped into the diluted HF solution (0.1 M) for one min at room temperature. After that, the substrates were rinsed with DI water and then dried by gentle N_2 gas. Finally, the HF-treated Si wafers were then in a vacuum vessel.

Fabrication of Si Nanowire Arrays

Procedures of HF/HNO_3 process with the assistance of Ag nano-seeds consists of two basic steps. The first step was performed by loading of Ag on Si substrates by dipping substrates into the mixed solutions containing $AgNO_3$ (0.005 M) and HF (4.5 M) for few seconds. In the second step, the as-prepared samples was rinsed with DI water and followed by drying with N_2 gas. Subsequently, the Ag-loaded Si wafers were immersed in the aqueous mixtures with various concentrations of HNO_3 (0.6-2.4 M) and 4.8 M of HF. The possible electrochemical reactions are listed as follows,

Cathodic reaction: [7]

$HNO_3 + 3H^+ \rightarrow NO + 2H_2O + 3h^+$

$HNO_3 \rightarrow HNO_2 \rightarrow NO \rightarrow HNO \rightarrow H_2N_2O_2 \rightarrow N_2O$

Anodic reaction:

$Si + 6F^- \rightarrow SiF_6^{2-} + 4e^-$

After rinsing with DI water several times, the residual Ag nanoparticles were removed completely by dipping the as-prepared samples in a concentrated HNO_3 (65%) solution for 2 min.

For comparing the etching rates of three different Ag^+-ion containing oxidants, 0.02 M of each oxidant was subsequently dissolved in 4.5 M of HF solution by magnetic stirring for 20 min, respectively. The involving dissolution reactions are presented as bellow,

$AgNO_3 \rightarrow Ag^+ + NO_3^-$

$Ag_2O + 2H^+ \rightarrow 2Ag^+ + H_2O$

$CH_3CO_2Ag + H^+ \rightarrow Ag^+ + CH_3CO_2H$

Characterizations

Morphologies of as-prepared nanowires were characterizations using field emission scanning electron microscopy (SEM, LEO 1530) observations. Surface coverage of Ag seeds was evaluated using the software, ImageJ, for processing the image analysis, where the recorded images were taken from the top-view SEM photographs of Ag-loaded samples. To characterize the wetting properties of nanowire arrays, the contact angle measurements of a drop of water were performed by a Rame-Hart goniometer equipped with a charge-coupled device camera.

Results and discussion

HF/HNO_3 Etching with Assistance of Ag

The process flow of conducting anisotropic etching with Ag-assisted HF/HNO_3 process is illustrated in Fig. 1(a). Briefly, in the first step, Ag nanoparticles were electrolessly deposited onto Si wafers through the galvanic displacement. After rising with distilled (DI) water several times and then drying with gentle N_2 flow, the Ag loaded Si samples were dipped into mixed aqueous solutions containing various concentration of HNO_3 (0.6-2.4 M) and 4.8 M of HF at room temperature. In this second process, each Ag nanoparticle acted as a microscopic cathode that initiated the redox process of dissociated HNO_3 for injecting holes into Si. The possible electrochemical reactions are summarized in the experimental section.

Meanwhile, Si atoms underneath the Ag seeds experienced the local oxidation reaction derived by the injected holes, and the oxidized Si was subsequently dissolved in HF etchants, leading the remaining oxide-free Si exposed to the next recycling reaction. Notice that the volume ratio of HNO_3 to HF was utilized in the range of 0.14 to 0.60, which is extremely lower than that of common used HNA process (normally above 3).[8,9] In such condition, dissolution of Si is no longer to be kinetically controlled by the oxide removal due to the utilization of abundant HF for processing. Instead, different from the typical HNA etching where the generated holes from cathodic reaction spatially separated on Si surfaces, the local dissolution of Si is more likely taken place beneath Ag seeds rather than the entire Si that exposes to the aqueous reactants. These phenomena imply that the charge transfer process dominates the etching mechanism of Ag-assisted HF/HNO_3 process, standing for the highly efficient transport pathway of carriers right between the electrolytes and Si.

On the other hand, with the assistance of Ag, the occurrence of HF/HNO_3 etching fundamentally resembles the reported two-steps MaCE process while H_2O_2 oxidants were used. Nevertheless, the distinct characteristics are visualized that distinguish the present method with H_2O_2-based MaCE reaction.[10] In the electrochemical aspect, the redox potential of H_2O_2 (E^0= +1.76 V) is comparably larger than both the Ag^+/Ag (E^0= +0.80 V) and NO_3^-/NO (E^0= +0.96 V) related oxidative reactions. This makes the thermodynamically favorable decomposition and redosposition of original Ag seeds during the catalytic dissolution of Si, resulting in the substantial difficulty on well controlling the surface features of etched structures. In fact, recent literatures have revealed the fact that the porosification of Si on etched nanowires may take place on H_2O_2-based MaCE.[11,12] More importantly, the dissociation preference of Ag is remarkably diminished in Ag-assisted HF/HNO_3 process due to the comparable potentials on reducing Ag and HNO_3, which allows the shape-maintenance of Ag nano-seeds during long-term catalytic movement within Si, functioning the uniform and kinetically stable etching of Si in a controllable manner.

Figures 1(b)-1(d) summarize the etching morphologies of Si (100) substrates under Ag-assisted HF/HNO_3 process with various concentrations of HNO_3 from 0.6, 1.2 to 1.8 M, respectively. With low concentrations of HNO_3 at 0.6 M, vertically aligned Si nanowires were formed, where the Ag seeds experienced the catalytic dissolution of Si exist at the Si nanowire/bulk interfaces, as shown in Fig. 1(b). Also, one can clearly find the existence of extremely smooth top surfaces of etched nanowire arrays upon 40-min process, which can be further evidenced in the insert of Fig. 1(b). Microstructures of the etched nanowires were further examined by HRTEM (high resolution transmission electron microscope) investigation, indicating that an as-prepared nanowire possesses {100} crystallographic configurations, as shown in the Electronic Supplementary Information. In addition to the uniform increase of nanowire lengths with adding the

This journal is © The Royal Society of Chemistry [year]

concentration of HNO_3 to 1.2 M, the consistent feature in terms of smooth topography of nanowires remains, as demonstrated in Fig. 1(c). These distinct phenomena, in contrast to the H_2O_2-based process where the rough nanowires were formed, as shown in the Electronic Supplementary Information, are mainly attributed to the lower reduction potential of nitrate ions provided for Si oxidation and dissolution. In other words, stable supply of holes from nitrate ions maintains the uniform movement of Ag seeds sinking into Si, and thereby leaves the smooth etched nanowires. These characteristics are expected to benefit the efficient reduction of undesired surface scattering of light when operating them as a light-trapping structure, which may benefit the development of high performance Si solar cells.[13,14] Notice that the formation of uneven top surfaces of etched nanowires can be found while the involved concentration of HNO_3 rises toward 1.8 M [Fig. 1(d)], owing to the intensive reaction derived by the concentrated HNO_3 through the substantial injections of holes into Si.

It has been reported that the roughness of nanostructure surfaces significantly correlates with their wetting characteristics, which can be readily understood by the model of Cassie–Baxter relation,[15]

$$\cos\theta_{CB} = r_{\Phi} f \cos\theta - r_{\Phi}(1-f) \quad (1)$$

where θ_{CB} and θ are the contact angle (CA) of nanostructured and polished Si surfaces, respectively, r_{Φ} is the roughness of the wetted area and *f* represents the area fraction of the solid-liquid interfaces on nanostructured Si surfaces. The examinations of wetting angles of fabricated nanowires through Ag-assisted HF/HNO_3 etching involved various amounts of HNO_3 are demonstrated in Fig. 2(a). Accordingly, contact angle measurements were conducted on the as-prepared samples before and after surface modification with PFOS (perfluorooctyl trichlorosilane). For comparison, we also performed the similar test on the nanowire sample prepared with 1.2M of H_2O_2-based MaCE. The measured results are summarized in Fig. 2(a), where the contact angles of nanowire surfaces all demonstrate the superhydrophilic properties with contact angle below 5^0. These results can be attributed to the appearance of surface oxide and rough topography of as-prepared samples. In addition, the HF/H_2O_2 etched sample possesses the most hydrophilic feature due to its comparably rough surfaces. Interestingly, after surface modification with low surface-energy PFOS molecules, the surface wettability turns to be superhydrophobic, with gradual increase of CA from 150^0-163^0 ($\pm 0.4^0$) by increasing the HNO_3 oxidants from 0.6-2.4 M, and approaches 170^0 ($\pm 0.2^0$) of CA using 1.2 M of H_2O_2 oxidants. The increased CA is directly associated with the introduction of surface roughness, as supported by the Equation 1. These results explicitly reveal the fact that the nanowires prepared with Ag-assisted HF/HNO_3 etching possess the comparably smooth topographies in comparison with samples treated using H_2O_2-based MaCE process. Furthermore, these findings also correspond well to the transitions of nanowire morphologies observed from SEM investigations, as found in Figs. 1(b)-1(d).

Kinetic Study

To further reveal the involving kinetics of Si dissolution via Ag-assisted HF/HNO_3 process, the length evolution of nanowires on reaction time along with various HNO_3 concentrations were examined, as displayed in Fig. 2(b). Apparently, the resulting nanowire lengths all demonstrate the linear relationship with etching time from each tested condition, which allows the well process controllability of Ag-assisted HF/HNO_3 etching for practical applications. Specifically, it can be concluded that the increased nanowire lengths correspond to the faster etching rates while the concentrated HNO_3 was involved in conducting the etching process. Parallel to unveiling the correlation of nanowire length versus etching time, another critical factor affecting reaction kinetics is process temperature. Figure 2(c) displays the temperature dependence of etching rate in logarithm term against the inverse form of reaction temperature. Moreover, the involving activation energy of each catalytic etching process can be evaluated following the Arrhenius equation,[16,17]

$$R = A\exp(-E_a/RT) \quad (2)$$

where R and A represent the etching rate of Si and pre-exponential factor, respectively. E_a, R and T are the activation energy, gas constant and reaction temperature, respectively.

Given the tested temperatures in the range of 25-50^0C, the corresponded E_a are found to be 47.3 ± 0.02 eV (using 1.2 M HNO_3), 38.3 ± 0.02 eV (using 1.8 M HNO_3), 36.5 ± 0.03 eV (using 2.4 M HNO_3), respectively. Likewise, the E_a of emerging 1.2 M of H_2O_2-based MaCE for etching is estimated to be 31.2 ± 0.05 eV. Since the removal of Si oxide is rather effective due to the utilization of abundant HF (4.8 M), the dissolution of Si is therefore limited by the number of holes injected to the valence band of Si for initiating the Si oxidation. Therefore, with higher concentration of HNO_3 oxidants, the hole injections can be more efficient, giving rising to the lower activation energy that responses to the energy barrier for the oxidization of Si. These kinetic features account for the fact that the etching of Si is dominantly determined by the oxidative reaction in both the Ag-assisted HF/HNO_3 and H_2O_2-based MaCE process, where the comparisons of etching rate at various temperatures are summarized in Fig. 2(d). It is found that the etching rate at each temperature is in rational accordance with the value of extracted E_a. Together with investigations of time factors in Fig. 2(b), it is validated that the involving process of Ag-assisted HF/HNO_3 process is dominantly determined by the oxidative reaction rather than the diffusion of reactive electrolytes.

Etching Dependence on Si Orientations

In this section, the dependence of Ag-assisted HF/HNO_3 process on crystallographic orientation of Si crystals was examined, as shown in Figs. 3. Interestingly, the distinct etching phenomena can be found on Si (111) substrates using an Ag-assisted HF/HNO_3 etching, where the as-prepared nanowires possess the one-dimensional zigzag morphologies rather than straight shapes. Instead, the smooth top surfaces of formed zigzag nanowires are still preserved [Fig. 3(a)], which validate the similar characteristic with the etching on Si (100) substrates, i.e., uniform movement of Ag seeds during the oxidation and dissolution of Si atoms. Meanwhile, despite there exhibits different numbers of transition node on zigzag nanowires ranging from 0 to 5, as presented in Fig. 3(b), each segment between nodes of formed nanowires stays in <100> directions. These gathered features imply the fact that Ag-assisted HF/HNO_3 etching holds the kinetically stable

electrochemical reaction with Si and preferentially maintains the <100> oriented etching on both Si (100) and (111)-crystal substrates. Likewise, the similar examination of orientated nanowires was performed on Si (110) wafers, as presented in Fig. 4(a). By carefully scratching the formed Zigzag nanowires and spraying them on a cleaned Si substrate, the associated slanted angles was unveiled, showing 90^0 of angle between two Si segments, as evidenced in the insert of Fig. 4(a). In addition, the orientation of formed nanowires can be further examined from the top-view SEM image, as shown in Fig. 4(b). It can be found that all nanowires orderly align to two principle directions with included angle of 90^0, which correspond to the crystallographic lattices of Si<100> orientations, as depicted in the insert of Fig. 4(b). Compared with nanowires prepared on Si (111), the majority of nanowire morphology is single-transition zigzag nanowires. By contrast, other multiple-transition conditions were rarely found, which may be attributed to the comparably large slanted angles of nanowires formed on (110) substrates.

These striking phenomena involve with the origin of transition nodes occurred in zigzag nanowires, especially for the frequent orientation transformation of zigzag nanowires formed on etching Si (111), which was rarely reported in MaCE-related researches.[18] Recent studies from K. Peng have regarded the autonomous motion of an Ag particle in Si by dynamically transforming the electrochemical energy to mechanical energy, suggesting the fact that the Ag catalysts enable to spontaneously move within Si without applying external bias.[19] In light of this finding, it is believed that the self-motivated moment of Ag nanoparticles can be driven by the additional thermodynamic factor, i.e., instant concentration change of reactant, at given temperature. It has been reported that the Ag catalysts possess the slight electrode activity for electrocatalytic reduction of nitrate ions.[20] Therefore, in addition to acting as oxidants for proceeding the directional etching on Si, the competitive pathway for consuming nitrate ions is accomplished by the electrocatalytic reduction initiated on Ag surfaces. Such electrocatalytic process, however, is only occurred at the exposed Ag surfaces in contact with electrolyte solutions rather than the entire surfaces of Ag catalysts. Considering that both of these competitive processes take place on Ag catalysts, the instant concentration of nitrate ions is locally changed at the exposed Ag surfaces. These combined effects generate the inhomogeneous electrochemical bias for driving the slight motion of Ag within Si, thus leading to the occurrence of zigzag nanowires, where the evolution of nanowire formation on various oriented wafers is illustrated in Fig. 4(c).

Apart from the kinetic visualization of Ag-assisted HF/HNO_3 etching, it is also pivotal to compare the currently reported method with other MaCE-related process. So far, one-step MaCE process, involved with $AgNO_3$ and HF as etchants, is considered a dominant etching technique for the controllable preparation of various Si nanostructures, varied from distinct microstructures, dimensions and orientations.[5,21] Recently, the underlying mechanism has been intensively investigated in both thermodynamic and kinetic ways.[21] In this process, the essential route of Si oxidation is generally believed to the supplement of Ag^+ reduction from $AgNO_3$ reagents, which not only creates the nanosized redox centers through the formation of primary Ag seeds, but further sustains the succeeding dissolution of Si from catalytic reduction of more Ag ions. These features hold true for the dominant oxidation process of Si, but the alternative pathway, supplied by the reduction of NO_3^- ions, has never been critically considered yet. With the detailed study of Ag-assisted HF/HNO_3 etching on Si addressed above, it is found that NO_3^- ions also behave as oxidants for injecting holes to the Si due to the more negative reduction potential than the valance band of Si. Accompanied with spontaneous reduction of both Ag^+ and NO_3^- ions, the process of Si dissolution can take place more efficiently, giving rise to the increased etching rate on Si.

This conclusion can be further supported by the comparisons of average etching rate with various Ag^+-ion containing reagents, as presented in Fig. 5(a). Three sets of experiments were performed under the similar condition except the presence of $AgNO_3$, Ag_2O and $AgC_2H_3O_2$ as oxidants, respectively. Following the corresponding reactions presented in the experimental section, it can be expected that the dissociation of 1 mol of Ag_2O in HF solution generates 2 mol of Ag ions, whereas 1 mol of Ag ions is provided using similar concentration of either $AgNO_3$ or $AgC_2H_3O_2$. It has been reported that the etching rate in MaCE positively correlates with current density (j) of associated redox process, expressed as below,[22]

$$j = -zek_cn_sC_{redox}\exp(-U/k_BT) \quad (3)$$

where z represents the number of transferred electrons. e, k_c and n_s are the charge of electrons, rate constant of redox process, electron density at the Si/electrolyte interface, respectively. C_{redox} corresponds to the concentration of Ag^+ ions. U and k_B are the activation energy and Boltzmann constant, respectively. According to Equation 3, the increase of concentration of Ag^+ ions (C_{redox}) involved in Si dissolution proportionally responses to the value of j due to more hole injections to the valence band of Si. Compared with the average etching rate of three tested oxidants, it can be clearly found that the resulting etching rate of Ag_2O oxidants approaches two times larger than that of $AgC_2H_3O_2$ oxidants [Fig. 5(a)], which corresponds well with the prediction of Equation 3, where the current density of redox process is dominantly supplied by the reduction of Ag ions. However, using $AgNO_3$ as oxidants results in the average etching rate (rate= 266 nm/min) approximately 1.3 times than that of $AgC_2H_3O_2$ (rate= 192 nm/min), as demonstrated in Fig. 5(a). Although the underlying reaction is hardly giving an intuitive visualization, this increased etching rate again evidences that NO_3^- ions also takes place in the oxidation of Si in $HF/AgNO_3$ aqueous system.

To gain insight into the involving electrochemical kinetics, a schematic examination of the charge transport process across the Si/Ag/etchants interface is displayed in Fig. 5(b), where the energy band diagrams show the situations before and after immersion of p-type silicon into $HF/AgNO_3$ electrolytes. When a p-type Si is brought in contact to the etching electrolytes, bending of the conduction and valence bands occurs in the vicinity of the interfaces to equilibrate the Fermi energy level in Si. Subsequently, the formation of Ag metal on Si surfaces spontaneously takes place by capturing the electrons from Si owing from its comparably lower redox potential than the energy level of valence band in Si. The result of Ag deposition leads to a reduced energy barrier that further facilitates the hole-injection through the Ag/Si contact, making a unidirectional migration of

This journal is © The Royal Society of Chemistry [year]

holes from electrolytes to Si. With the accumulation of holes at Ag/Si interfaces, the interfacial charges constitute the currents flowing from the local cathode (Ag) toward the anodic sites (Si), guiding more holes to participate in and thereby initiate the dissolution of Si. In HF/$AgNO_3$ electrolyte system, the reduction of both NO_3^- and Ag are energetically favorable, because the corresponding energies of redox reaction (-5.20 eV in Ag^+/Ag; -5.36 eV in NO_3^-/NO) are much negative than the valence band of Si coated with Ag. Thus, the interplay of hole injections from Ag^+ an NO_3^- ions, supplied by the $AgNO_3$ precursors, collectively contributes to the efficient dissolution of Si, leaving the formation of Si nanowires afterward.

Formation of Straight Si Nanowires on Si (111)

Despite the diversified morphologies of nanowire arrays can be formed using Ag-assisted HF/HNO_3 process, a reliable strategy that is capable of regularizing the orientation of etched nanowires on non-Si (100) wafers is in highly demand.[23] To attain the control over the nanowire morphology, we started from engineering the distribution of electrolessly deposited Ag seeds on Si. As shown in Fig. 6(a), the direct loading of Ag onto Si (111) for 30s leads to the formation of discrete Ag nanoparticles. As detailed in the experimental section, by treating the cleaned Si (111) wafers with diluted HF (0.1 M) for a minute prior to Ag loading, the nucleated Ag seeds turn to be closely interconnected, as shown in Fig. 6(b). With longer Ag deposition up to 45s on HF-pretreated Si substrates, the increased surface coverage of formed Ag seeds was displayed with consistent interconnection [Fig. 6(c)]. The pretreatment of HF essentially removed the native oxide existed on Si surfaces, and further passivated them with the formation of Si-H termination. Such surface configuration occurred on Si facilitates the subsequent nucleation of Ag seeds through electroless deposition due to the creation of preferred wetting of Si in contact with electrolytes. The summarized results in terms of deposition time versus surface coverage of Ag seeds are presented in Fig. 6(d). It can be found that the coverage of Ag in area ratio can be abruptly increased over 80% upon HF-pretreated Si wafers at a given Ag-loading time. Moreover, these results provide the universal guideline of tuning the deposition coverage of Ag on Si, not only allows the better morphological controllability of Ag-assisted HF/HNO_3 process, but further benefits the applications of nanostructured Ag on photonic[24] and biomedical[25] fields.

We further performed the Ag-assisted HF/HNO_3 etching on Si (111) substrates with turned coverage of Ag deposition. Apparently, distinct etching morphologies can be found on the bare Si [Fig. 7(a)] and HF-treated Si [Fig. 7(b)] with 30s of Ag deposition. It appears that the zigzag nanowires were formed on bare Si wafers, as demonstrated in the insert of Fig. 7(a), whereas the dissolution of Si takes place vertically throughout relative to the substrate plane of HF-treated Si wafers [insert of Fig. 7(b)]. Such remarkable transition of oriented nanowires can be interpreted by the distinct distribution of Ag catalysts, where the interconnected Ag seeds were sank into Si together and thereby forced to etch Si (111) vertically, leaving the straight and well-aligned nanowires afterward. Notice that there is no obvious dissolution of Si can be found on the bare Si wafers while applying etching process without Ag seeds, as presented in Fig. 7(c), which clearly distinguishes the present method from conventional HNA techniques. Finally, the comparisons of etching rate on three oriented Si substrates are displayed in Fig. 7(d), which indicate the uniform etching rates on the prepared Si substrates with Ag deposition, regardless of wafer orientations of Si.

Conclusions

In conclusion, we explored the new designed HF/HNO_3 etching with the assistance of Ag for the preparation of diversified Si nanostructure arrays with extremely smooth top surfaces at room temperature. The remarkable transition of Si etching can be resulted in, from the fully isotropic features (using conventional HNA process) to the one-dimensional configurations (using Ag-assisted HF/HNO_3 process). With systematical investigations on structural characterizations, surface wettability, time and temperature dependent kinetics, the involving mechanism was visualized, where the local hole injections from NO_3^- ions to Si through Ag seeds function the kinetically uniform and stable etching of Si in a controllable manner. By engineering the Ag deposition on Si, the area coverage of electrolessly deposited Ag can be well modulated, offering the sound controllability of nanowire morphologies on various orientated Si substrates. These new strategic technique, combined with in-depth kinetic investigations, not only allow the better understanding of wet chemical etching methods, but further benefit many practical applications, particularly in solar cells, nanophotonic devices and biological/medical platforms.

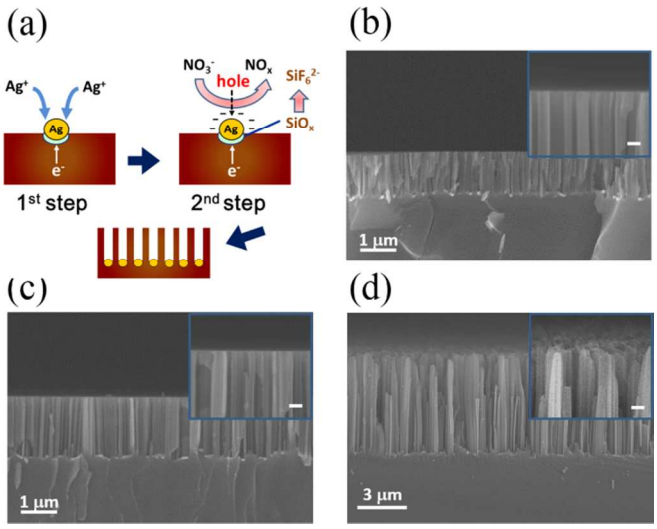

Fig. 1 (a) Illustrations of two-steps process flow of conducting anisotropic etching with Ag-assisted HF/HNO_3 process (b) Cross-sectional SEM images of resulting nanowire arrays preapred with 4.8 M of HF and various HNO_3 concentrations: (b) 0.6 M, (c) 1.2 M and (d) 1.8M. The corresponding high-magneifcation SEM images are presented in the insert figures, revealing the existance of extremely smooth top surfaces in the insert figure of both Figs. 1(b) and 1(c), whereas the rough morphologies can be found in the insert figure of Figure 1(d). The scale bars are 200 nm in the insert figures.

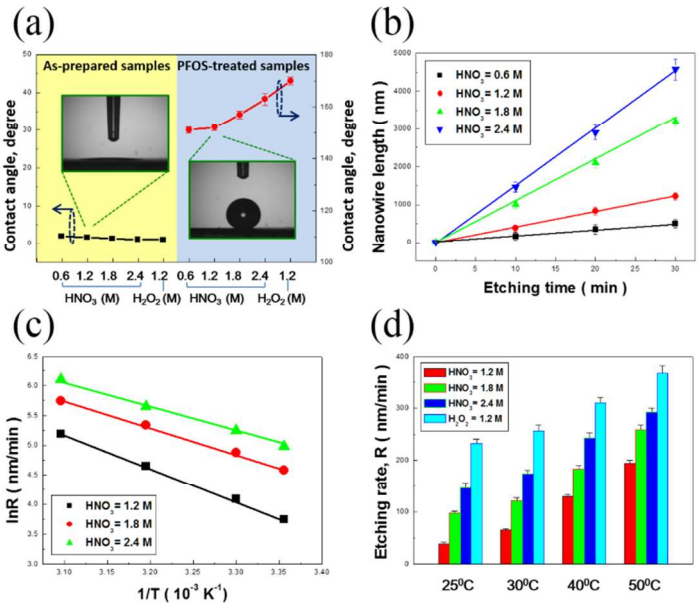

Fig. 2 (a) Contact angle measurements of as-prepared Si nanowire arrays (left) and PFOS-treated samples (right) prepared with various etching conditions, respectively. (b) Plot of etching time verus lengths of etched nanowires obtained using four different concentrations of HNO_3 oxidants. (c) Relationship of etching rate (in logarithm term) and reaction temperature (in inverse term) of three prepared nanowire arrays. (d) Summarized comparisons of nanowire's etching rate fabricated with HF/HNO_3 and HF/H_2O_2 electrolytes within the temperature region of 25^0C-50^0C, respectively.

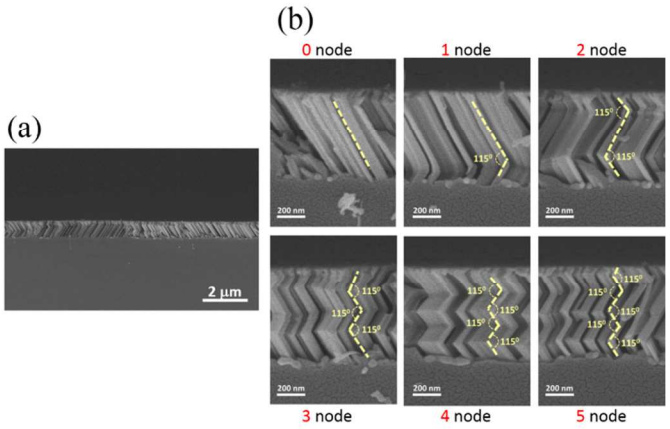

Fig. 3 (a) Cross-sectional SEM image of etching result on Si (111) substrates using Ag-assistd HF/HNO_3 process. Notice that the smooth top surfaces remains, similarly with the etching features formed on Si (100) substrates. (b) Six different zigzag morphologies with numbers of transition node from 0 to 5 on an individual nanowire, respectively. The included angle of each nanowire segment is confirmed to be 115^0 consistently, verifying the fact that those zigzag nanowires are all along <100> directions.

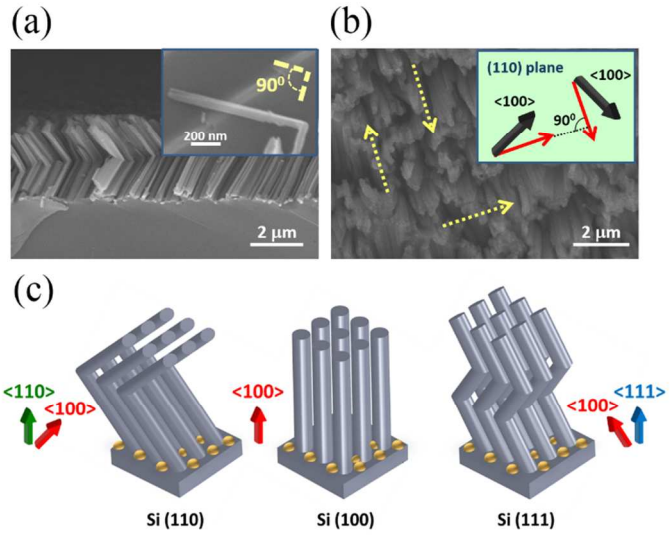

Fig. 4 (a) Cross-sectional SEM image of nanowire arrays on Si (110) substrates prepared with Ag-assistd HF/HNO_3 process. A single scretched nanowire with two vertially aligned segments is presented in the insert figure. (b) Top-view SEM image of etched arrays with three principle orientated axes denoted with yellow arrows. The insert figure further presents the projection of those axes to the Si (110) plane, which are corresponded to the crystallographic lattices of Si<100> orientations. (c) Schematic evolution of nanowire formation on three various oriented wafers.

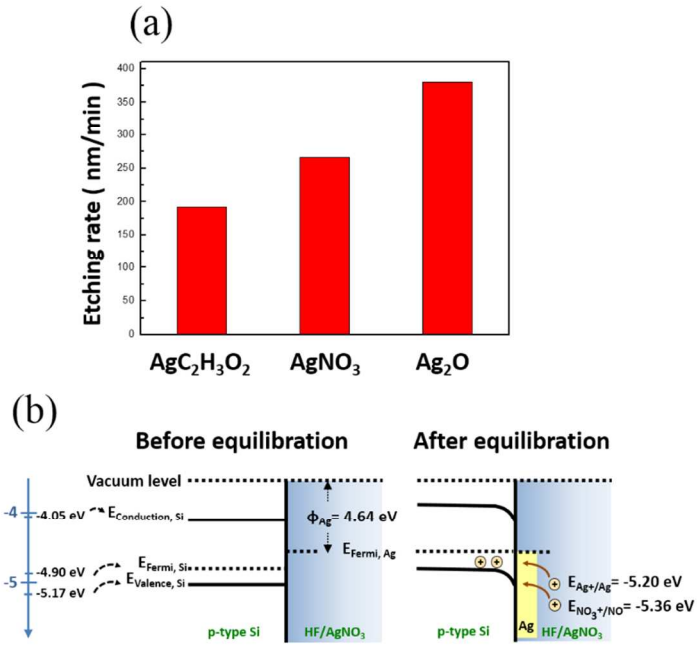

Fig. 5 (a) Comparisons of average etching rate using three different Ag^+-ion based oxidants. (b) Energy band diagrams before and after equilibration while immersing p-type silicon into $HF/AgNO_3$ electrolytes.

This journal is © The Royal Society of Chemistry [year]

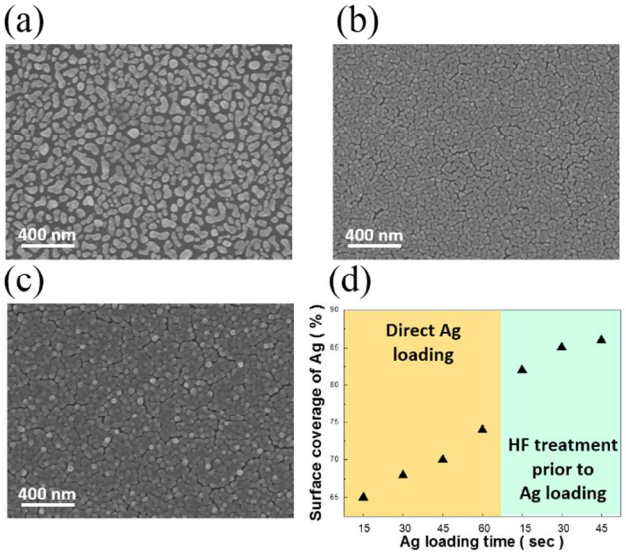

Fig. 6 Top-view SEM images of Ag-loaded Si (111) wafers under following conditions: (a) 30s of direct Ag loading without performing the pretreatment on Si (111) substrates, (b) 30s of Ag loading on Si (111) substrates treated with diluted HF solution and (c) 45s of Ag loading on Si (111) substrates treated with diluted HF solution. Clearly, the discrete Ag nanoparticles can be found in Fig. 6(a), whereas the closely interconnected Ag seeds were occurred in both Figs. 6(b) and 6(c). (d) Summarized results in terms of deposition time versus surface coverage of Ag seeds.

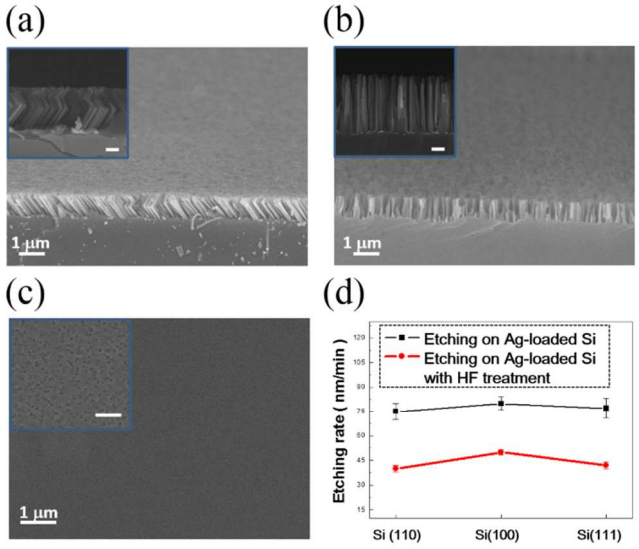

Fig. 7 30^0-tilt SEM images of etching results on (a) bare Si (111) and (b) HF-treated Si (111) with 30s of Ag deposition. The insert figures reveal the distinct nanowire morphologies in these two cases, while the similar smooth top surfaces maintain regardless of preparation methods of Ag loading. (c) Top-view SEM image of Si (111) wafers after dipping in HF/HNO_3 electrolyte solutions for 2 hr without loading the Ag seeds on Si substrates prior to etching process. The corresponding high-magnification SEM image is demonstrated in the insert figure, where only tiny nano-pits with average size less than 20 nm can be observed. Evidently, the comparisons of Figs. 7(a)-(c) unveil the explicit distinction between the present Ag-assisted HF/HNO_3 method with conventional HNA techniques. The scale bars are 200 nm in the insert figures. (d) Summarized results of etching rate on three oriented Si substrates. Meanwhile, etching rates on Ag-loaded Si with and without HF treatments are incorporated. The comparably smaller deviations and values of etching rate from HF-treated Si exist in three oriented Si wafers, in comparison with bare Si under direct deposition of Ag prior to etching process.

Acknowledgments

The work is financially supported by Ministry of Science and Technology, Taiwan (MOST 103-2218-E-260-001-).

Notes and references

[a] *Department of Applied Materials and Optoelectronic Engineering, National Chi Nan University, No.1, Daxue Rd., Puli Township, Nantou County 545, Taiwan. Email: timcychen@ncnu.edu.tw*
[b] *School of Materials Science and Engineering, Georgia Institute of Technology, 771 Ferst Drive NW, Atlanta, Georgia 30332, United States.*
[c] *Faculty of Engineering, The Chinese University of Hong Kong, Shatin, Hong Kong, China*
† Electronic Supplementary Information (ESI) available: See DOI: 10.1039/b000000x/

1. K. W. Kolasinski, *Curr. Opin. Solid State Mater. Sci.* **2005**, *9*, 73.
2. X. Li, *Curr. Opin. Solid State Mater. Sci.*, 2012, **16**, 71.
3. (a) C. T. Seo, C. H. Bae, D. S. Eun, J. K. Shin and J. H. Lee, *Jpn. J. Appl. Phys.*, 2004, **43**, 7773; (b) G. T. A. Kovacs, N. I. Maluf and K. E. Petersen, *Proc. IEEE*, 1998, **86**, 1536.
4. H. Robbins and B. Schwartz, *J. Electrochem. Soc.*, 1959, **106**, 505.
5. (a) K. Q. Peng, Y. J. Yan, S. P. Gao and J. Zhu, *Adv. Mater.*, 2002, **14**, 1164; (b) K. Q. Peng, J. J. Hu, Y. J. Yan, Y. Wu, H. Fang, Y. Xu, S. T. Lee and J. Zhu, *Adv. Funct. Mater.*, 2006, **16**, 387; (c) C. Y. Chen, W. J. Li, H. H. Chen, *ChemPhysChem*, 2012, **13**, 1415; (d) W. K. To, C. H. Tsang, H. H. Li and Z. Huang, *Nano Lett.*, 2011, **11**, 5252; (e) J. Liu and Z. Huang, *J. Phys. Chem. C*, 2014, **118**, 17870.
6. (a) O. J. Hildreth, D. Brown and C. P. Wong, *Adv. Mater.*, 2011, **21**, 3119; (b) A. I. Hochbaum, R. Chen, R. D. Delgado, W. Liang, E. C. Garnett, M. Najarian, A. Majumdar and P. Yang, *Nature*, 2008, **451**, 163; (c) W. K. To, J. Fu, X. Yang, V. A. L. Roy and Z. Huang, *Nanoscale*, 2012, **4**, 5835.
7. (a) E. S. Kooij, K. Butter and J. J. Kelly, *Electrochem. Solid-State Lett.*, 1999, **2**, 178; (b) M. Steinert, J. Acker and K. Wetzig, *J. Phys. Chem. C*, 2008, **112**, 14139.
8. S. Liu, C. Palsule, S. Yi and S. Gangopadhyay, *Phys. Rev. B*, 1994, **49**, 10318.
9. A. A. Hamzah, N. A. Aziz, B. Y. Majlis, J. Yunas, C. F. Dee and B. Bais, *J. Micromech. Microeng.*, 2012, **22**, 095017.
10. (a) C. Chartier, S. Bastide and C. L. Clement, *Electrochim. Acta*, 2008, **53**, 5509; (b) J. Yeom, D. Ratchford, C. R. Field, T. H. Brintlinger and P. E. Pehrsson, *Adv. Funct. Mater.*, 2014, **24**, 106; (c) S. Chang, V. P. Chuang, S. T. Boles and C. V. Thompson, *Adv. Funct. Mater.*, 2010, **20**, 4364.
11. X. Zhong, Y. Qu, Y. C. Lin, L. Liao and X. Duan, *ACS Appl. Mater. Interfaces*, 2011, **3**, 261.

12. (a) C. Chiappini, X. Liu, J. R. Fakhoury and M. Ferrari, *Adv. Funct. Mater.,* 2010, **20**, 2231; (b) Y. Qu, H. Zhou and X. Duan, *Nanoscale*, 2011, **3**, 4060.
13. E. Garnett and P. Yang, *Nano Lett.,* 2010, **10**, 1082.
14. K. Q. Peng, X. Wang, L. Li, X. L. Wu and S. T. Lee, *J. Am. Chem. Soc.,* 2010, **132**, 6872.
15. Y. Xiu, L. Zhu, D. W. Hess and C. P. Wong, *J. Phys. Chem. C,* 2008, **112**, 11403.
16. S. L. Cheng, C. H. Chung and H. C. Lee, *J. Electrochem. Soc.*, 2008, **155**, D711.
17. Z. Huang, N. Geyer, P. Werner, J. Boor and U. Gosele, *Adv. Mater.*, 2011, **23**, 285.
18. V. A. Sivakov, G. Bronstrup, B. Pecz, A. Berger, G. Z. Radnoczi, M. Krause and S. H. Christiansen, *J. Phys. Chem. C,* 2010, **114**, 3798.
19. K. Q. Peng , A. Lu , R. Zhang and S. T. Lee , *Adv. Funct. Mater.,* 2008, **18**, 3026.
20. (a) M. Fedurco, P. Kedzierzawski and J. Augustynskia, *J. Electrochem. Soc.*, 1999, **146**, 2569; (b) M. A. Bhat, P. P. Ingole, V. R. Chaudhari and S. K. Haram, *New J. Chem.*, 2009, **33**, 207.
21. (a) K. Q. Peng, H. Fang, J. J. Hu, Y. Wu, J. Zhu, Y. J. Yan and S. T. Lee, *Chem. Eur. J.*, 2006, **12**, 7942; (b) C. Y. Chen, L. Li and C. P. Wong, *Chem. Asian J.*, 2014, **9**, 93.
22. (a) J. Kim, Y. H. Kim, S. H. Choi and W. Lee, *ACS Nano*, 2011, **5**, 5242; (b) N. Mitsugiz and K. Nagai, *J. Electrochem. Soc.*, 2004, **151**, G302.
23. H. E. Jeong, I. Kim, P. Karam, H. J. Choi and P. Yang, *Nano Lett.*, 2013, **13**, 2864.
24. R. A. Puebla, L. M. L. Marzan and F. J. G. de Abajo, *J. Phys. Chem. Lett.*, 2010, **1**, 2428.
25. X. M. Qian and S. M. Nie, *Chem. Soc. Rev.*, 2008, **37**, 912.

This journal is © The Royal Society of Chemistry [year]